Available online at www.sciencedirect.com
ScienceDirect
C. R. Mecanique 337 (2009) 385–394
COMPTES RENDUS MECANIQUE

Combustion for aerospace propulsion

Massively parallel LES of azimuthal thermo-acoustic instabilities in annular gas turbines

P. Wolf [a,*], G. Staffelbach [a], A. Roux [a], L. Gicquel [a], T. Poinsot [b], V. Moureau [c]

[a] *CERFACS, 42, avenue G. Coriolis, 31057 Toulouse cedex 1, France*
[b] *IMFT – CNRS, Toulouse, France*
[c] *Turbomeca (SAFRAN group), Bordes, France*

Available online 21 July 2009

Abstract

Increasingly stringent regulations and the need to tackle rising fuel prices have placed great emphasis on the design of aeronautical gas turbines, which are unfortunately more and more prone to combustion instabilities. In the particular field of annular combustion chambers, these instabilities often take the form of azimuthal modes. To predict these modes, one must compute the full combustion chamber, which remained out of reach until very recently and the development of massively parallel computers. In this article, full annular Large Eddy Simulations (LES) of two helicopter combustors, which differ only on the swirlers' design, are performed. In both computations, LES captures self-established rotating azimuthal modes. However, the two cases exhibit different thermo-acoustic responses and the resulting limit-cycles are different. With the first design, a self-excited strong instability develops, leading to pulsating flames and local flashback. In the second case, the flames are much less affected by the azimuthal mode and remain stable, allowing an acceptable operation. Hence, this study highlights the potential of LES for discriminating injection system designs. ***To cite this article: P. Wolf et al., C. R. Mecanique 337 (2009).***

Résumé

SGE massivement parallèle des instabilités thermo-acoustiques azimutales dans les turbines à gaz annulaires. La conception des turbines à gaz aéronautiques est aujourd'hui de plus en plus délicate avec souvent l'apparition d'instabilités de combustion. Pour prédire ces instabilités, qui prennent fréquemment la forme de modes azimutaux dans les chambres annulaires, il est nécessaire de simuler l'intégralité de la chambre, ce qui restait hors de portée jusqu'à très récemment et l'apparition des calculateurs massivement parallèles. Cet article présente les Simulations aux Grandes Echelles (SGE) de deux chambres d'hélicoptère complètes qui ne diffèrent que sur certains détails géométriques des tourbillonneurs. Dans les deux cas, la SGE capture l'apparition et l'établissement de modes azimutaux tournants. Néanmoins, les deux cas présentent des réponses thermo-acoustiques différentes et les cycles limites correspondants diffèrent. Pour l'un des cas, une forte instabilité se développe et entraîne une pulsation des flammes tandis que l'autre cas montre des flammes qui restent bien ancrées et nettement moins affectées par le mode. Cette étude souligne donc la capacité de la SGE à discriminer des systèmes d'injection. ***Pour citer cet article : P. Wolf et al., C. R. Mecanique 337 (2009).***

Keywords: Fluid dynamics; Combustion instabilities; Annular gas turbines; Azimuthal modes; LES

Mots-clés : Mécanique des fluides ; Instabilités de combustion ; Turbines à gaz annulaires ; Modes azimutaux ; SGE

* Corresponding author.
E-mail address: pierre.wolf@cerfacs.fr (P. Wolf).

1631-0721/$ – see front matter
doi:10.1016/j.crme.2009.06.003

1. Introduction

More than eighty percent of the energy produced worldwide is created by combustion of fossil fuels that has severe effects on the environment and is greatly responsible for global climate change. Moreover, the fuel resources are dramatically decreasing. Combined to the fact that nowadays there is no real substitute to combustion for many applications such as aeronautical engines, optimizing the process of combustion is the key answer to controlling those issues. To enhance combustion implies new designs and operating ranges for engines, usually by using lean combustion. Unfortunately, these technological choices lead to combustion instabilities that often take the form of azimuthal modes in annular gas turbines [1–4]. Strong coupling of acoustics and non-linear heat release results in thermo-acoustic instabilities that can appear as both standing or rotating modes [5].

To predict and avoid these modes requires a deeper understanding of the underlying physics governing the stability of annular gas turbines. Experimental studies require full test rigs, which are costly and rare. Numerically, the study and prediction of annular chamber stability can be achieved by using one-dimensional networks [6,7] or Helmholtz solvers [8,9]. However these methods rely on the concept of the flame transfer function, which remains a key element and needs to be evaluated or modeled using Large Eddy Simulation (LES) for example. Although LES could potentially predict combustion instabilities, its use was restrained to the modeling of the flame transfer function obtained on a single sector simulation. LES of the full combustion chamber stayed out of reach until very recently through the development of massively parallel computers. Today, full annular chambers can be computed on massively parallel machines by running LES codes on a thousand to several thousands of processors, producing real engine operating conditions and their thermo-acoustic stability.

Following a previous study by Staffelbach et al. [10] two helicopter engines, only differing on the design of the swirlers, are presented and compared. The first section describes the LES code and the models. The target configurations are then exposed, before presenting the LES results that help discriminating these two designs in terms of thermo-acoustic instabilities.

2. LES and numerical models

LES is known to be able to predict reacting flows [4,11,12], stability of flames [13] and the flame-acoustic interaction [14,15]. In this paper, a fully compressible unstructured explicit code is used to solve the reactive multi-species Navier–Stokes equations [16–18]. A third order finite element scheme is used for both time and space advancement [19]. Sub-grid stress tensor is modeled by a classical Smagorinsky approach [20]. Boundary conditions are implemented through the NSCBC formulation [21,22] and wall boundaries use a logarithmic wall-law approach [15].

Chemistry is computed by means of a reduced one-step mechanism for JP-10/air flames, JP-10 being a surrogate for kerosene. This mechanism is fitted to match the full scheme behaviour for equivalence ratio between 0.4 and 1.5 [23]. Five species are explicitly transported and solved: JP10, O_2, CO_2, H_2O and N_2. To better capture flame/turbulence interactions, the Dynamic Thickened Flame (DTF) model is used. The baseline idea of the DTF model is to detect reaction zones using a sensor and to thicken only these reaction zones, leaving the rest of the flow unmodified. Thickening depends on the local grid resolution and it locally adapts the combustion process to reach a numerically resolved flame front. The flame sub-grid scale wrinkling and interactions at the SGS level are supplied by an efficiency function [24,25].

3. Target configurations

Two variants of an annular helicopter gas turbine are computed in this study. Versions A and B only differ on the swirlers' design, the combustion chamber itself remains the same and is equipped with fifteen burners. Each swirler consists of two co-annular counter-rotating swirl stages. Differences between version A and B are geometrical, the separator between inner and outer swirling stages has a different shape, as shown in Fig. 2.

The whole chamber is computed with its casing, which helps avoiding uncertainties on the boundary conditions. Indeed, the calculated domain starts immediately after the compressor's outlet, where inlet profiles are known, and extends to a chocked nozzle corresponding to the throat of the high pressure distributor (Fig. 1). Fuel is supposed to be totally vaporized and only gaseous phase is computed to simplify the LES. Air inflow is at 578 K and feeds the

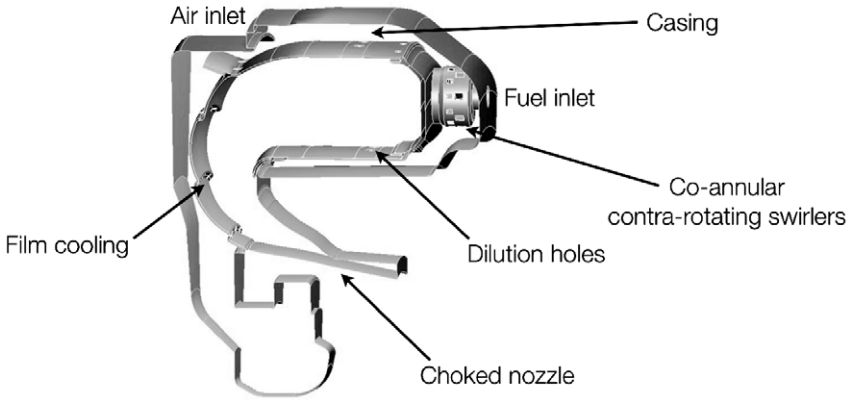

Fig. 1. Boundary conditions and geometry shown on a single sector.

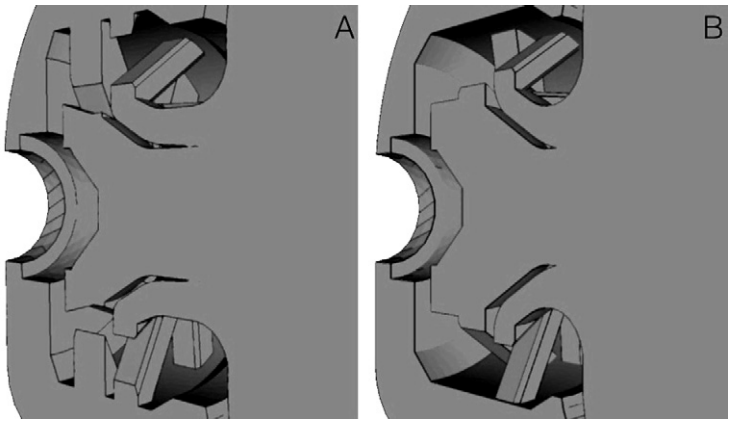

Fig. 2. View of the swirlers. Left and right correspond to versions A and B, respectively.

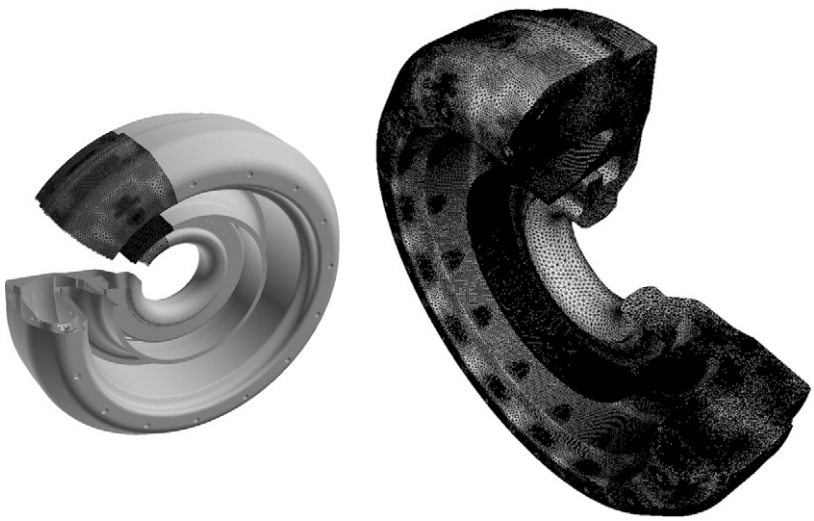

Fig. 3. View of the combustion chamber and mesh.

combustion chamber through the swirlers, cooling films and dilution holes. Multi-perforated walls used to cool the liners are taken into account by a homogeneous boundary condition [26].

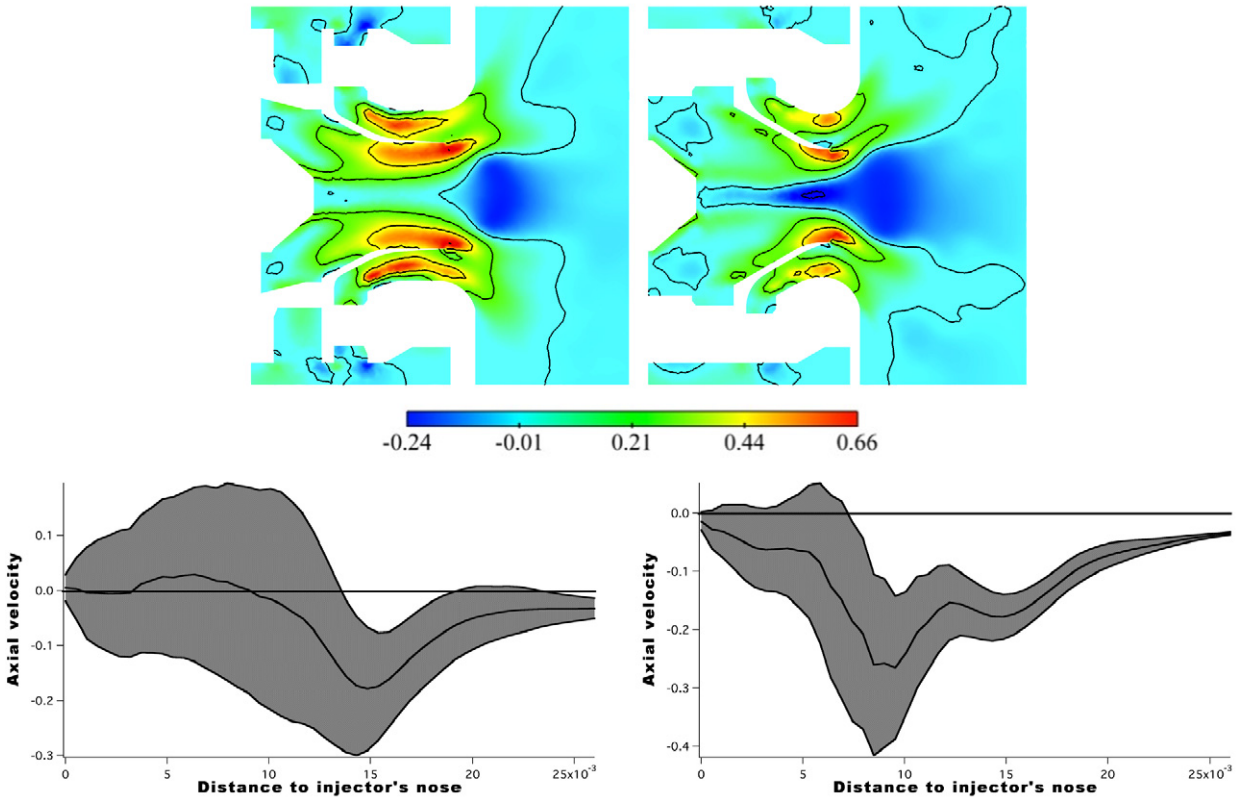

Fig. 4. Axial velocity fields obtained with a non-reactive atmospheric pressure LES (top). Axial velocity envelope on the swirler's axis (bottom). Left and right correspond to versions A and B, respectively. Velocities are normalized by the bulk velocity.

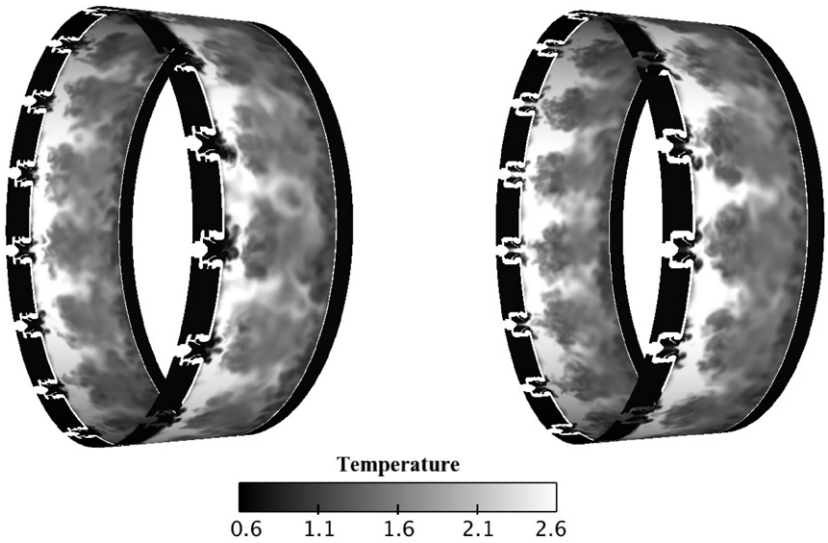

Fig. 5. Temperature field on a cylindrical plane containing the swirlers' axis. Left and right correspond to versions A and B, respectively. Values are normalized by mean temperature.

The final full annular mesh for version A is made of 9,009,065 nodes and 42,287,640 tetrahedral elements. Typical time step for this configuration is 7.5×10^{-8} seconds. The version B mesh contains 6,916,125 nodes and 37,696,365 tetrahedral elements and has a typical time step of 5.9×10^{-8} seconds. The initial conditions for versions A and B

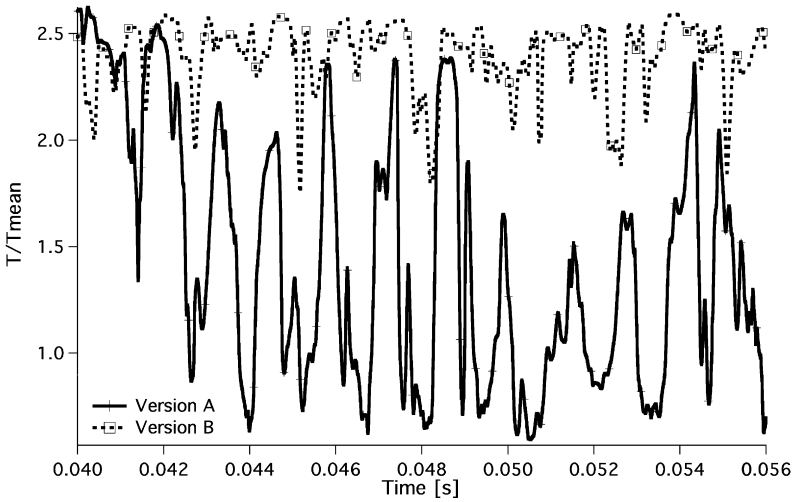

Fig. 6. $\frac{T}{T_{mean}}$ over time at swirler's exit for versions A and B.

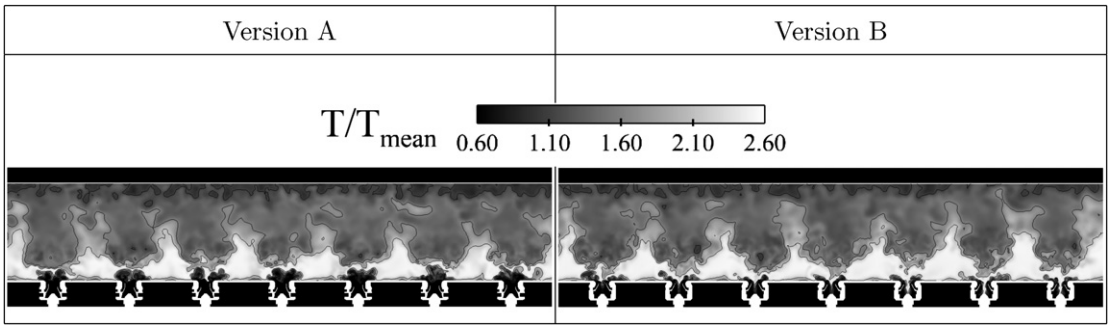

Fig. 7. Temperature fields with temperature isocontours at a given instant on the developed surface of a cylinder containing the swirler's axis for half the burners. The left and right columns correspond, respectively, to versions A and B. Values are normalized by mean temperature.

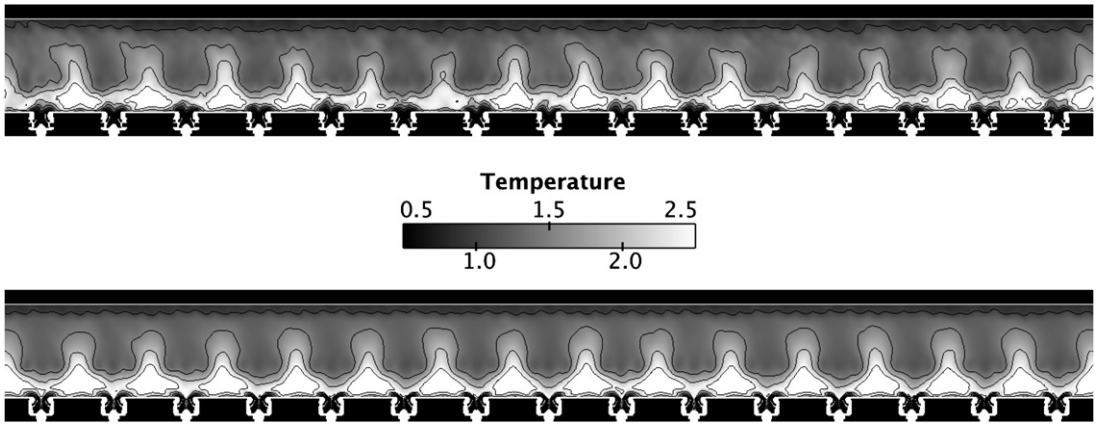

Fig. 8. Time-averaged temperature fields on a developed surface of a cylinder containing the swirler's axis for all burners for version A (top) and B (bottom). Values are normalized by mean temperature.

are obtained from statistically converged single sector LES with periodic boundary conditions that are azimuthally duplicated fourteen times (Fig. 3). In the following, each of the fifteen burners is numbered starting with sector 1 placed at $z = 0$ and $y > 0$ and increasing clockwise.

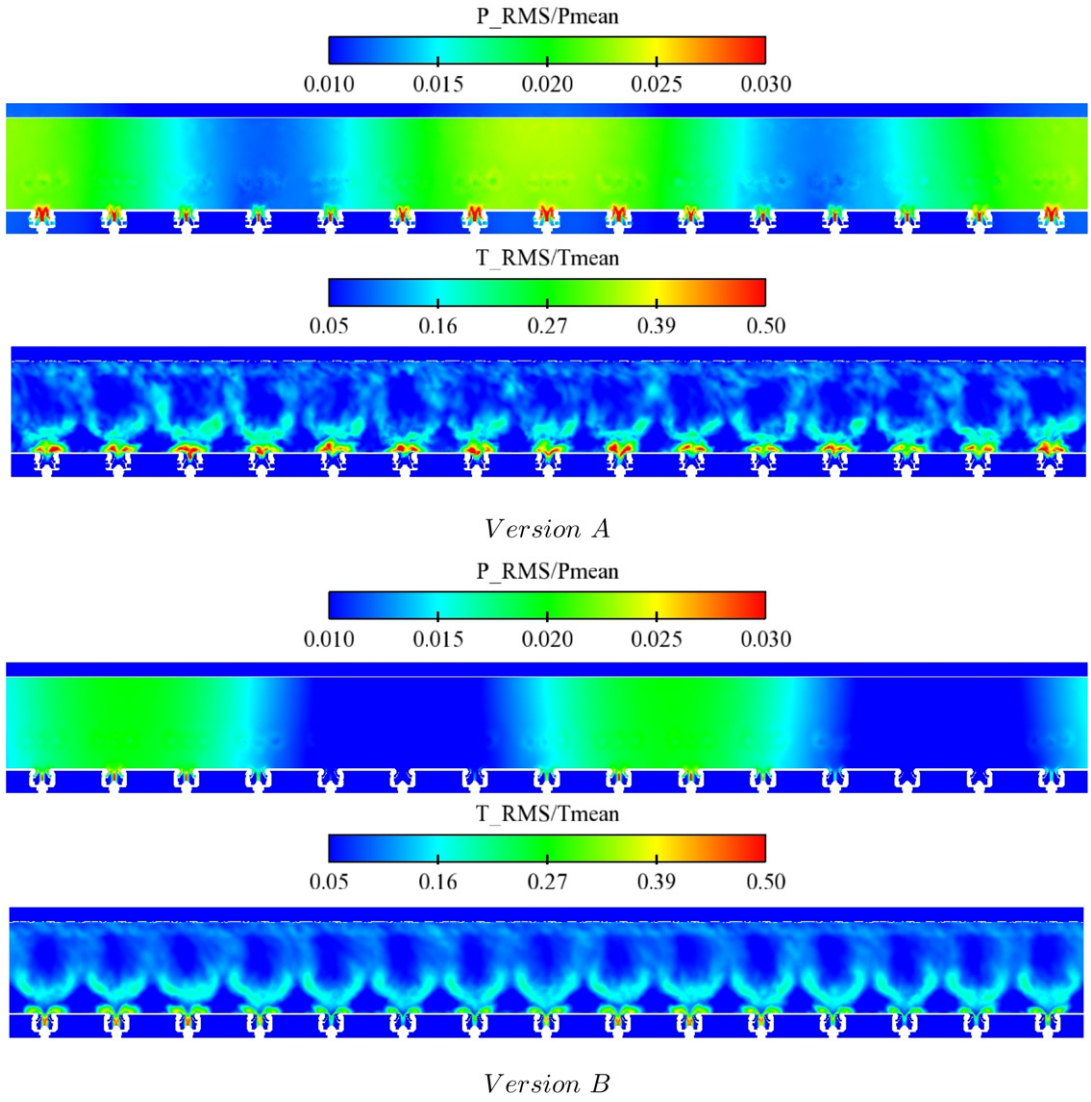

Fig. 9. Developed surface of a cylinder containing the swirler's axis for all burners. From top to bottom: Pressure and temperature fluctuation levels for versions A and B.

4. LES of two helicopter engines

LES of the non-reacting flows within the two swirlers have first been obtained to apprehend the potential differences induced by the geometrical changes and before investing into massively parallel LES of the two engines. An observation of the axial velocity fields obtained for these non-reactive atmospheric pressure LES, Fig. 4, reveals a strong recirculation zone positioned along the injector's axis of symmetry and which enters the inner passage of version B. Version A also yields a recirculation zone centered along the swirler's axis of symmetry. This structure, however, remains in the chamber and does not enter the injector contrarily to version B predictions. These behaviours are confirmed by plotting the mean axial velocity profile supplemented by the local value of its RMS to define the envelope of variations of this quantity, Fig. 4. Results are then shown as a function of the axial distance to the swirler's end wall along the swirler's axis of symmetry, Fig. 4. The wider envelope for version A implies stronger fluctuations of the axial velocity when compared to version B. These results suggest very different flame anchoring mechanisms and sensitivities to acoustic perturbations, confirmed by the full annular reactive LES discussed hereafter.

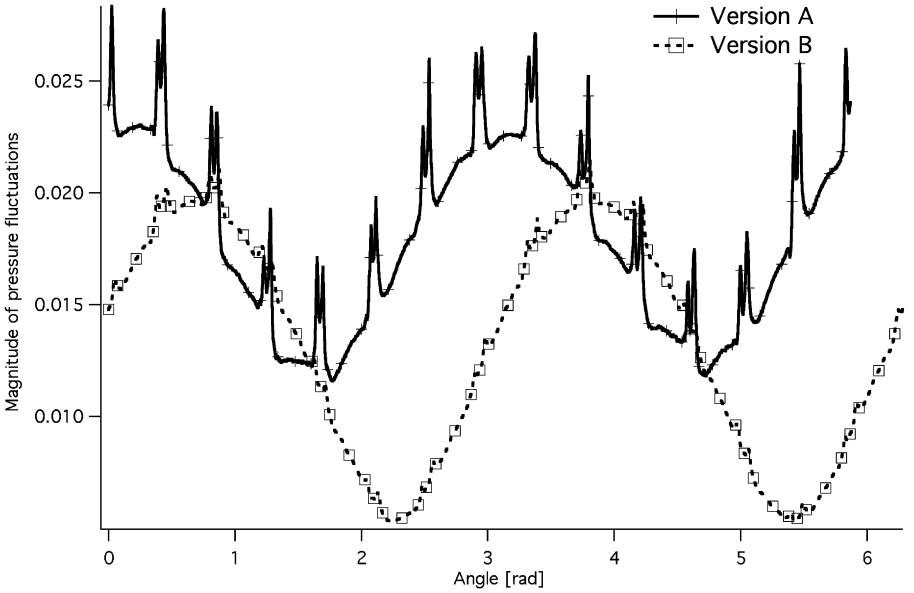

Fig. 10. Magnitude of normalized pressure fluctuations $\frac{P_{RMS}}{P_{mean}}$ on a line passing by all burners' axis for versions A and B.

Versions A and B have been run on 2048 processors on a SGI Altix Ice 3 equipped with Intel Xeon 3 GHz CPUs. LES of 0.1 seconds physical time required around 400,000 CPU hours corresponding to 196 hours of execution time. Fig. 5 shows snapshots of the temperature field on a cylindrical plane containing the swirler's axis for versions A and B. An observation of this field versus time (not presented here) shows that, in both cases, the flames oscillate azimuthally and axially with time. The oscillation is more pronounced for version A with visible strong fluctuations of the flame position. That behaviour is not observed in version B predictions. Note that B type swirlers' recirculating zone topology leads to flame that are anchored upstream very close to the injector's outlet. Fig. 6 presents the temporal evolution of temperature at the swirler's exit and confirms that version A flames strongly move back and forth, whereas version B flames remain anchored close to the injector's lips. Fig. 7 provides a better insight of this phenomenon by showing instantaneous temperature fields on a developed surface that corresponds to the cylinder of Fig. 5 at a given instant but only for part of the full annular chamber. An observation of the pressure fluctuation fields versus time (not shown here) clearly reveals the propagating azimuthal pressure waves for both versions. As these waves meet the flames, the latter move back and forth as well as from left to right.

Fig. 8 shows the time-averaged temperature fields for versions A and B. The flames present very different mean shapes. A flames have more perturbed flame fronts whereas B flames all exhibit V shaped fronts. B type swirlers provide clean and stable recirculation zones in front of each burner allowing a steady anchoring region for the flames. On the contrary, A type swirlers generate unstable recirculating zones imposing strong flow variations to the flames which result into large local heat-release fluctuations.

Fig. 9 presents the time-averaged pressure and temperature fluctuations: $\frac{P_{RMS}}{P_{mean}}$ and $\frac{T_{RMS}}{T_{mean}}$ for versions A and B on the developed surface of Fig. 8. The azimuthal development of the RMS pressure fields indicates two zones of high fluctuations separated by two relatively calm zones in both cases. Version B presents much less pressure fluctuations when compared to case A, demonstrating that the amplitude of the pressure wave is smaller for version B [10].

The differences in pressure variations are confirmed by Fig. 10 where $\frac{P_{RMS}}{P_{mean}}$ is plotted for both cases along a line contained in the developed surface and located in front of all burners' exits. Fig. 10 shows higher maximum magnitude of pressure fluctuations for version A and much lower minimum values for version B. Note also that fifteen local peaks appear on the pressure profile for version A predictions. These strong local variations coincide with the fifteen burners for which flame positioning is not stable enough and explains such levels of fluctuations. Such peaks can barely be observed for version B, indicating that this injection system is much more stable and much less sensitive to acoustic forcing. Note that such a statement can be quantified though the evaluation of the integrated value of the pressure RMS profiles provided in Fig. 10. That is, 121.538 and 79.913 for versions A and B respectively: i.e. a 34% reduction of

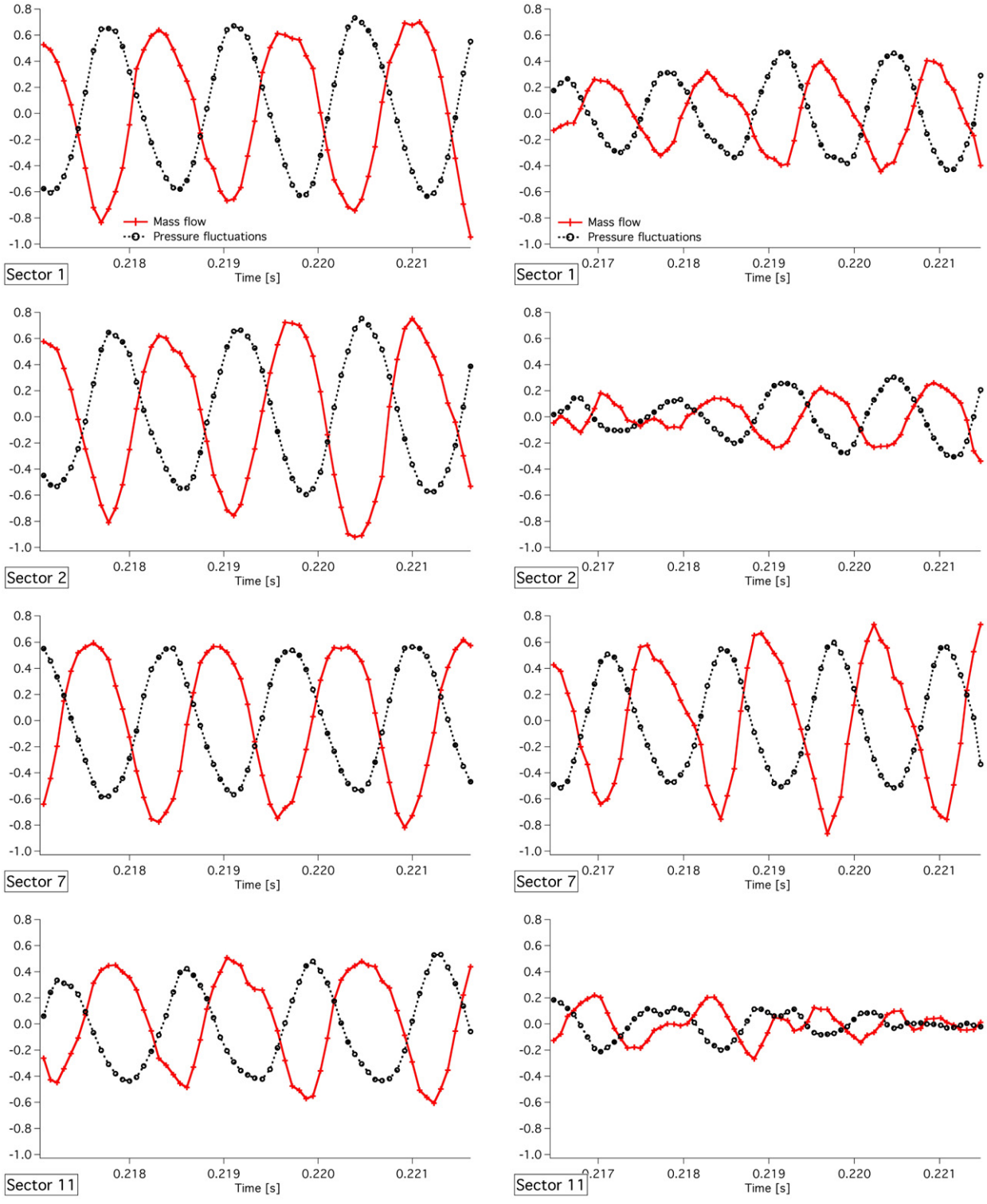

Fig. 11. Swirler mass flow rates and pressure fluctuations over time for sectors 1, 2, 7 and 11.

the pressure activity. Most of the reduction is for this diagnostic due to one factor: type A swirlers provide a pressure RMS field with no quiet zone and large amplitude variations. All burners of that chamber are subject to acoustic pressure fluctuations. Such a behaviour is explained by the superposition of two contra-rotating waves with one mode containing more energy than the other [1–4,10]. Type B chamber, on the other hand, has several burners subject to almost no acoustic forcing. This indicates the presence of two equal energy containing contra-rotating waves resulting into the first azimuthal eigenmode of the system.

One mechanism evidenced in version A simulations and potentially at the source of the strong self-sustained oscillating operating point, is the acoustic forcing of the mass-flow rate through each burner [10]. Indeed such variations will impact the mixing of fuel with air prior to its combustion inside the chamber, as well as the hydrodynamic stability of the recirculation zone positioned in front of each swirler. These flow rate fluctuations can then perturb combustion, which can feed the thermo-acoustic instability loop. This assumption is corroborated by Fig. 11, which shows pressure fluctuations and mass flow rates through the swirlers for different sectors. Mass flow rate and pressure are normalized as:

$$\bar{\dot{m}}^* = \frac{\dot{m} - \dot{m}_{average}}{\dot{m}_{average}}, \qquad \bar{P}^* = \frac{P - P_{average}}{\Delta P}$$

(where ΔP is the overall pressure loss of the chamber). Fig. 11 reveals sinusoidal fluctuations of pressure and mass flow rate for all sectors and for both versions. Mass flow rate and pressure are linked: when the pressure is minimum, the mass flow rate through the swirlers is maximum and inversely. This general mechanism is observed for both cases and all sectors. Case B, however, evidences sectors where the amplitude of these fluctuations is strongly reduced (see for example sectors 2 and 11 in Fig. 11) with time contrarily to case A. Such behaviour confirms the fact that the structure of the instability is somewhat different between versions A and B. Indeed, in both cases, two contra-rotating waves are superposed, but one is clearly predominant for version A [10] whereas the amplitudes of the modes are similar when considering case B. Thus, the strongest fluctuations for version B are located on the sectors where the two waves meet. Note that low Mach number effects induce slightly different propagating speeds of these two waves ($u + c$ and $u - c$), yielding the low frequency time-evolution of the fluctuations: fluctuations in sectors 1, 2 and 7 are getting stronger with time while sector 11 is becoming softer.

5. Conclusion

LES of two versions of a full annular helicopter combustion chamber were performed using massively parallel computations. Both cases reveal self-established azimuthal acoustic modes. The resulting rotating pressure waves perturb the flames axially and azimuthally. These waves also modulate the mass flow rate through the swirlers. However, the two cases are found to present different thermo-acoustic responses and one case demonstrates a much quieter operation than the other one. Thus, the potential of LES for discriminating injection systems and predict stability of combustion chambers is highlighted.

Acknowledgements

The authors thank GENCI (Grand Equipement National de Calcul Intensif) as well as CINES (Centre Informatique National de l'Enseignement Superieur) for providing the computer power necessary for these simulations.

References

[1] C.O. Paschereit, B. Schuermans, P. Monkewitz, Non-linear combustion instabilities in annular gas-turbine combustors, in: 44th AIAA Aerospace Sciences Meeting and Exhibit, 2006.

[2] S. Candel, Combustion instabilities coupled by pressure waves and their active control, in: 24th Symp. (Int.) on Combustion, The Combustion Institute, Pittsburgh, 1992, pp. 1277–1296.

[3] D.G. Crighton, A.P. Dowling, J.E. Ffowcs Williams, M. Heckl, F. Leppington, Modern Methods in Analytical Acoustics, Lecture Notes, Springer-Verlag, New York, 1992.

[4] T. Poinsot, D. Veynante, Theoretical and Numerical Combustion, 2nd edition, R.T. Edwards, 2005.

[5] T. Lieuwen, V. Yang, Combustion instabilities in gas turbine engines. Operational experience, fundamental mechanisms and modeling, in: Progress in Astronautics and Aeronautics, vol. 210, AIAA, 2005.

[6] U. Krueger, J. Hueren, S. Hoffmann, W. Krebs, P. Flohr, D. Bohn, Prediction and measurement of thermoacoustic improvements in gas turbines with annular combustion systems, in: ASME Paper, ASME TURBO EXPO, Munich, Germany, 2000.
[7] S.R. Stow, A.P. Dowling, Thermoacoustic oscillations in an annular combustor, in: ASME Paper, New Orleans, Louisiana, 2001.
[8] F. Nicoud, L. Benoit, Global tools for thermo-acoustic instabilities in gas turbines, in: APS/DFD Meeting, Bull. Amer. Phys. Soc., vol. 48, New York, 2003.
[9] F. Nicoud, L. Benoit, C. Sensiau, T. Poinsot, Acoustic modes in combustors with complex impedances and multidimensional active flames, AIAA Journal 45 (2) (2007) 426–441.
[10] G. Staffelbach, L.Y.M. Gicquel, G. Boudier, T. Poinsot, Large Eddy Simulation of self excited azimuthal modes in annular combustors, Proceedings of the Combustion Institute 32 (2) (2009) 2909–2916.
[11] F. Di Mare, W.P. Jones, K. Menzies, Large eddy simulation of a model gas turbine combustor, Combustion and Flame 137 (2004) 278–295.
[12] H. Pitsch, Large eddy simulation of turbulent combustion, Annual Review of Fluid Mechanics 38 (2006) 453–482.
[13] A. Sengissen, J.F. Van Kampen, R. Huls, G. Stoffels, J.B.W. Kok, T. Poinsot, Les and experimental studies of cold and reacting flows in a swirled partially premixed burner with and without fuel modulation, Combustion and Flame 150 (2007) 40–53.
[14] L.Y.M. Gicquel, Y. Sommerer, B. Cuenot, T. Poinsot, LES and acoustic analysis of turbulent reacting flows: Application to a 3D oscillatory ramjet combustor, in: ASME 2006, Paper AIAA-2006-151, Reno, USA, 2006.
[15] P. Schmitt, T.J. Poinsot, B. Schuermans, K. Geigle, Large-eddy simulation and experimental study of heat transfer, nitric oxide emissions and combustion instability in a swirled turbulent high pressure burner, Journal of Fluid Mechanics 570 (2007) 17–46.
[16] G. Boudier, L.Y.M. Gicquel, T. Poinsot, D. Bissières, C. Bérat, Comparison of LES, RANS and experiments in an aeronautical gas turbine combustion chamber, Proceedings of the Combustion Institute 31 (2007) 3075–3082.
[17] S. Roux, G. Lartigue, T. Poinsot, U. Meier, C. Bérat, Studies of mean and unsteady flow in a swirled combustor using experiments, acoustic analysis and large eddy simulations, Combustion and Flame 141 (2005) 40–54.
[18] G. Boudier, L.Y.M. Gicquel, T. Poinsot, Effect of mesh resolution on large eddy simulation of reacting flows in complex geometry combustors, Combustion and Flame 155 (2008) 196–214.
[19] O. Colin, M. Rudgyard, Development of high-order Taylor–Galerkin schemes for unsteady calculations, Journal of Computational Physics 162 (2) (2000) 338–371.
[20] J. Smagorinsky, General circulation experiments with the primitive equations: 1. The basic experiment, Monthly Weather Review 91 (1963) 99–164.
[21] T. Poinsot, S. Lele, Boundary conditions for direct simulations of compressible viscous flows, Journal of Computational Physics 101 (1) (1992) 104–129.
[22] V. Moureau, G. Lartigue, Y. Sommerer, C. Angelberger, O. Colin, T. Poinsot, Numerical methods for unsteady compressible multi-component reacting flows on fixed and moving grids, Journal of Computational Physics 202 (2) (2004) 710–736.
[23] J.-Ph. Légier, Simulations numériques des instabilités de combustion dans les foyers aéronautiques, Ph.D. thesis, INP Toulouse, 2001.
[24] O. Colin, F. Ducros, D. Veynante, T. Poinsot, A thickened flame model for large eddy simulations of turbulent premixed combustion, Physics of Fluids 12 (7) (2000) 1843–1863.
[25] J.-Ph. Légier, T. Poinsot, D. Veynante, Dynamically thickened flame LES model for premixed and non-premixed turbulent combustion, in: Proceedings of the Summer Program, Center for Turbulence Research, NASA Ames/Stanford Univ., 2000, pp. 157–168.
[26] S. Mendez, F. Nicoud, An adiabatic homogeneous model for the flow around a multi-perforated plate, AIAA Journal 46 (10) (2008) 2623–2633.